PRAMANA
— journal of
physics

Vol. 70, No. 5
May 2008
pp. 817–833

Microscopic insight in the study of yrast bands in selenium isotopes

PARVAIZ AHMAD DAR, SONIA VERMA, RANI DEVI* and S K KHOSA
Department of Physics and Electronics, University of Jammu, Jammu 180 006, India
*Corresponding author. E-mail: rani_rakwal@yahoo.co.in

MS received 30 March 2007; revised 19 October 2007; accepted 1 January 2008

Abstract. The yrast bands of even–even selenium isotopes with $A = 68$–78 are studied in the framework of projected shell model, by employing quadrupole plus monopole and quadrupole pairing force in the Hamiltonian. The oblate and prolate structures of the bands have been investigated. The yrast energies, backbending plots and reduced $E2$ transition probabilities and g-factors are calculated and compared with the experimental data. The calculated results are in reasonably good agreement with the experiments.

Keywords. Selenium isotopes; projected shell model; yrast bands; $B(E2)$ transition probability; g-factors.

PACS Nos 21.60.Cs; 21.10.Ky; 21.10.Re; 27.60.+e

1. Introduction

The study of selenium isotopes with $A = 68$–78 has been at the centre stage of nuclear physics for quite sometime in the past [1–41]. Substantial effort on the experimental side has been put to investigate the nuclear structure determining properties of these isotopes [1–31]. Presently, experimental data are available on energy spectra, $B(E2)$ transition probabilities, nuclear magnetic g-factors and quadrupole deformation parameters for these isotopes. For example, in ^{68}Se an oblate deformed ground state band has been observed up to $I^\pi = 10^+$ and was found to coexist with a prolate deformed excited band. In the first in-beam studies of ^{70}Se, low-lying states up to $I^\pi = 4^+$ were observed. The level scheme was later extended to $I^\pi = 8^+$ and rotational band built on the 0^+ ground state was observed. This band undergoes a band crossing in the spin region $I = 4 \rightarrow 8$. A systematic decrease of $B(E2)$ transition strengths with increasing spin in the same spin region has been observed which has been interpreted as the interaction between prolate and oblate structures. Very recently [13,14], experimental evidence is presented for the prolate shape for the 2_1^+ state in ^{70}Se re-opening the question as to whether there are, as reported earlier, deformed oblate shapes near to the ground state in

light selenium isotopes. The ground state band of ^{72}Se has been the subject of several experimental investigations [15–17]. Mylaeus *et al* [15] and Palit *et al* [16] have extended the yrast band up to spin 28^+. The transitional nucleus ^{72}Se is observed to feature a spectrum typical of shape coexistence. This interpretation is based on the rotational-like energy spacings of the yrast states with $I \geq 6$. Recently, the yrast band of ^{74}Se has been investigated up to $I^\pi = 22^+$ [18]. Earlier experiments [8] on ^{72}Se include lifetime measurements up to $I^\pi = 14^+$ state along the yrast band. A systematic increase of the $B(E2)$ values for the spin $I^\pi = 12^+$ has been observed in ^{72}Se contrary to the trend found in ^{74}Se. A recent study [18] of ^{74}Se shows a deformed shape for the excited states with a considerable softness towards triaxiality. With these varying projected shape evolutions at higher excited states in even–even selenium isotopes, the study of structure of high spin states through measurements of transition strengths in ^{72,74}Se would be of considerable interest. The band structures of ^{76,78}Se have been studied by the reaction ^{74,76}Ge$(\alpha, 2n\gamma)^{76,78}$Se using a variety of in-beam γ-ray techniques. Spin and parities have been assigned uniquely for many new levels in ^{76,78}Se. The yrast spectra in these isotopes have been obtained up to a spin of $10\hbar$ [22,23].

In contrast to the large experimental effort there are not many theoretical attempts that have been made to understand the complex excitation energy spectra of the Se isotopes [16–18,20,22,23,32–40]. In the case of ^{68}Se the self-consistent microscopic calculations with the projected Hartree–Fock [37] was used and found to have met limited success. Recently, projected shell model (PSM) [32] was used to explain the structure of excitation energy spectra in ^{68}Se. It is demonstrated that calculations with this model can achieve a comparable quality to the large-scale shell model diagonalizations. But the present model can be applied to much heavier isotopes. Rainovski *et al* [19] applied cranked Nilsson–Strutinsky [39] approach for the study of ^{70}Se nucleus. A fairly consistent description of the observed high-spin states in ^{70}Se was achieved by them. The structure of high-spin states was investigated earlier through microscopic calculations using the EXCITED VAMPIR model [38]. In these calculations the yrast states of low spin up to $I^\pi = 6^+$ appear to have mainly oblate character. For high spins, an oblate band coexists with many other prolate bands. Altogther six bands have been calculated up to $I^\pi = 22^+$. In the case of ^{74}Se, Hartree–Fock–Bogoliubov (HFB) cranking calculations were performed by Nazarewicz *et al* [40] to obtain an interpretation of the ground and excited state bands. The calculations suggest that without rotation the nucleus is quite soft in the gamma coordinate but has a weak oblate minima at $\epsilon_2 \sim 0.218$. The general characteristics of these calculations is the coexistence of two collectively rotating shapes at comparable binding energies which is consistent with the existence of two parallel rotating bands observed in ^{74}Se. The level structures of ^{76,78}Se have been calculated with the interacting boson model (IBM) [20,22,23]. The IBM had been known to describe well the collective states in the $A = 100$–200 region of nuclei and because of it this model has been applied successfully to ^{76,78}Se. Matsuzaki and Taketani [22] applied this model for the study of positive parity states in $^{74-78}$Se isotopes.

From the overview of the research input, it turns out that presently the excitation energy spectra in $^{68-74}$Se is available up to a spin of $I^\pi \simeq 28^+$ whereas in ^{76,78}Se the spectra is known up to $I^\pi = 12^+$. From the analysis of experimental data,

it turns out that these nuclei are transitional nuclei displaying some unexpected features. Besides a varying collectivity reflected by the $B(E2)$ values, they exhibit pronounced single particle and shell effects. These nuclei do not behave like good vibrators or good rotors. The ratio $E4/E2$ increases from 2.1 to 2.7 across the sequence of isotopes. Proton-rich as they may be called, exhibit phenomena that are quite unlike most heavy nuclei that have stable deformation. The structural changes are quite pronounced among neighbouring isotopes and this mass chain is often characterized by shape coexistence phenomena. The competition between proton and neutron shell gaps occurring at large oblate and prolate deformations near the neutron numbers 36 and 38 results in a coexistence of different nuclear shapes. The structure of these nuclei provides a good test for nuclear models. The test of the model in the true sense would be to check its reliability in reproducing the main features of the entire mass chain.

As pointed out earlier, many nuclear models have been invoked to study Se nuclei but their limitations have been that they have been applied to specific isotopes taking one or two isotopes at a time. It would be very interesting to see if a single calculational framework could be used for describing the entire mass chain of Se isotopes. Recently, projected shell model (PSM) [32] was used to explain the structure of excitation energy spectra in ^{68}Se. It was demonstrated that calculations with this model can achieve a comparable quality to the large-scale shell model diagonalizations. That is why we have chosen to apply this model to the proton-rich mass chain of Se isotopes.

2. Projected shell model

The detailed description of PSM can be found in review articles [42,43]. The PSM is based on the spherical shell model concept. It differs from the conventional shell model in that the PSM uses the angular momentum projected states as the basis for the diagonalization of the shell model Hamiltonian.

The wave function in the PSM is given by

$$|\sigma, IM\rangle = \sum_{K,\kappa} f_\kappa^\sigma \hat{P}^I_{MK} |\phi_\kappa\rangle. \tag{1}$$

The index σ labels the states with same angular momentum and κ the basis states. $\hat{P}^I_{MK}$ is the angular momentum projection operator and f_κ^σ are the weights of the basis states κ. We have assumed axial symmetry for the basis states and the intrinsic states are, therefore, the eigenstates of the K-quantum number. For calculations of an even–even system, the following four kinds of basis states $|\phi_\kappa\rangle$ are considered: the quasi-particle (qp) vacuum $|0\rangle$, two-quasi-neutron states $a^\dagger_{\nu 1} a^\dagger_{\nu 2}|0\rangle$ and two-quasi-proton states $a^\dagger_{\pi 1} a^\dagger_{\pi 2}|0\rangle$. For instance, $|0\rangle$ is the ground-state band (g-band) of an even–even nucleus.

The weight factors, f_κ^σ in eq. (1), are determined by diagonalization of the shell model Hamiltonian in the space spanned by the projected basis states given above. This leads to the eigenvalue equation

$$\sum_{\kappa'} (H_{\kappa\kappa'} - E_\sigma N_{\kappa\kappa'}) f^\sigma_{\kappa'} = 0, \tag{2}$$

and the normalization is chosen such that

$$\sum_{\kappa\kappa'} f^{\sigma}_{\kappa} N_{\kappa\kappa'} f^{\sigma'}_{\kappa'} = \delta_{\sigma\sigma'}, \tag{3}$$

where the Hamiltonian and norm-matrix elements are given by

$$H_{\kappa\kappa'} = \langle\phi_\kappa|\hat{H}\hat{P}^I_{K_\kappa} K'_{\kappa'}|\phi_{\kappa'}\rangle, \tag{4}$$

$$N_{\kappa\kappa'} = \langle\phi_\kappa|\hat{P}^I_{K_\kappa} K'_{\kappa'}|\phi_{\kappa'}\rangle. \tag{5}$$

Projecting an intrinsic state $|\phi_\kappa\rangle$ onto a good angular momentum generates the rotational band associated with this intrinsic configuration, whose rotational energy is given by the expectation value of the Hamiltonian as a function of spin I.

$$E_\kappa(I) = \frac{\langle\phi_\kappa|\hat{H}\hat{P}^I_{KK}|\phi_\kappa\rangle}{\langle\phi_\kappa|\hat{P}^I_{KK}|\phi_\kappa\rangle} = \frac{H_{\kappa\kappa}}{N_{\kappa\kappa}}. \tag{6}$$

A diagram in which rotational energies $E_\kappa(I)$ for various bands are plotted against spin I is referred to as a band diagram [42] which contains incredibly rich information. In the numerical calculations, we have used the standard quadrupole–quadrupole plus (monopole and quadrupole) pairing force, i.e.,

$$\hat{H} = \hat{H}_0 - \frac{1}{2}\chi\sum_\mu \hat{Q}^\dagger_\mu\hat{Q}_\mu - G_M\hat{P}^\dagger P - G_Q\sum_\mu \hat{P}^\dagger_\mu\hat{P}_\mu, \tag{7}$$

where $\hat{H}_0$ is the spherical single-particle Hamiltonian. The strength of the quadrupole force χ is adjusted such that the known quadrupole deformation parameter ϵ_2 is obtained. This condition results from the mean-field approximation of the quadrupole–quadrupole interaction of the Hamiltonian in eq. (7). The monopole pairing force constants G_M are adjusted to give the known energy gaps. For all the calculations, the monopole pairing strengths G_M used in the calculation are

$$G^\nu_M = \left[19.58 - 15.66\frac{N-Z}{A}\right]A^{-1}, \quad G^\pi_M = 19.58A^{-1}. \tag{8}$$

These strengths are taken from [32]. The strength parameter G_Q for quadrupole pairing is assumed to be proportional to G_M. In the present work, the proportionality constant G_Q is fixed as 0.22 for $^{68-78}$Se.

Electromagnetic transitions can give important information on the nuclear structure and provide a stringent test of a particular model. In the present work, we have calculated the electromagnetic properties using PSM approach. The reduced transition probability $B(EL)$ from the initial state $(\sigma_\mathrm{i}, I_\mathrm{i})$ to the final state $(\sigma_\mathrm{f}, I_\mathrm{f})$ are given by [44]

$$B(EL, I_\mathrm{i} \to I_\mathrm{f}) = \frac{e^2}{(2I_\mathrm{i}+1)}|\langle\sigma_\mathrm{f}, I_\mathrm{f}\|\hat{Q}_L\|\sigma_\mathrm{i}, I_\mathrm{i}\rangle|^2, \tag{9}$$

where the reduced matrix element is given by [44]

$$\langle \sigma_{\rm f}, I_{\rm f} \| \hat{Q}_L \| \sigma_{\rm i}, I_{\rm i} \rangle = \sum_{\kappa_{\rm i},\kappa_{\rm f}} f^{\sigma_{\rm i}}_{\kappa_{\rm i}} f^{\sigma_{\rm f}}_{\kappa_{\rm f}} \sum_{M_{\rm i},M_{\rm f},M} (-)^{I_{\rm f}-M_{\rm f}} \begin{pmatrix} I_{\rm f} & L & I_{\rm i} \\ -M_{\rm f} & M & M_{\rm i} \end{pmatrix} \times \langle \phi_{\kappa_{\rm f}} | \hat{P}^{I_{\rm f}}_{K_{\kappa_{\rm f}} M_{\rm f}} \hat{Q}_{LM} \hat{P}^{I_{\rm i}}_{K_{\kappa_{\rm i}} M_{\rm i}} | \phi_{\kappa_{\rm i}} \rangle$$

$$= 2 \sum_{\kappa_{\rm i},\kappa_{\rm f}} f^{\sigma_{\rm i}}_{\kappa_{\rm i}} f^{\sigma_{\rm f}}_{\kappa_{\rm f}} \sum_{M',M''} (-)^{I_{\rm f}-K_{\kappa_{\rm f}}} (2I_{\rm f}+1)^{-1} \begin{pmatrix} I_{\rm f} & L & I_{\rm i} \\ -K_{\kappa_{\rm f}} & M' & M'' \end{pmatrix} \times \int {\rm d}\Omega D_{M''K_{\kappa_{\rm i}}}(\Omega) \times \langle \phi_{\kappa_{\rm f}} | \hat{Q}_{LM'} \hat{R}(\Omega) | \phi_{\kappa_{\rm i}} \rangle. \quad (10)$$

The gyromagnetic factors (g-factors) $g(\sigma, I)$, $g_\pi(\sigma, I)$ and $g_\nu(\sigma, I)$ are defined by [44]

$$g(\sigma, I) = \frac{\mu(\sigma, I)}{\mu_N I} = g_\pi(\sigma, I) + g_\nu(\sigma, I) \quad (11)$$

with $g_\tau(\sigma, I)$, $\tau = \pi$, ν given by

$$g_\tau(\sigma, I) = \frac{1}{\mu_N [I(I+1)]^{1/2}} \times [g^\tau_l \langle \sigma, I \| \hat{J}^\tau \| \sigma, I \rangle + (g^\tau_s - g^\tau_l) \langle \sigma, I \| \hat{S}^\tau \| \sigma, I \rangle]. \quad (12)$$

The PSM calculations proceed in two steps. First an optimum set of deformed basis is constructed from the standard Nilsson model. The Nilsson parameters are taken from the N-dependent values in [45]. The present calculations are performed by considering three major shells ($N = 2$, 3 and 4) for both neutrons and protons. The basis deformation ϵ_2 is taken either according to experimental information or from total Routhian surface calculations [1,2,14,16,19,21,25]. We emphasize that, unlike cranking mean-field approaches, the deformation parameters used as an input to the PSM calculations need not correspond exactly to the true nuclear deformation. This is because of the shell model nature of the PSM: the deformed single-particle states serve solely as a way to truncate the shell model basis. All observable properties in the PSM calculations are determined by the many-body wave functions obtained by diagonalizing the shell model Hamiltonian. The chosen energy window around the Fermi surface gives rise to a basis space, $|\phi_\kappa\rangle$ in eq. (1), of the order of 67. In the second step, these basis states are projected to good angular momentum states, and the projected basis is then used to diagonalize the shell model Hamiltonian. The diagonalization gives rise to the energy spectra, and electromagnetic quantities are calculated by using the resulting wave functions.

In the present paper the energy window around the neutron and proton Fermi surfaces have been chosen to be 9.96 MeV for obtaining the two-quasi-neutron and two-quasi-proton basis states. For restricting the 4-qp configurations an energy window of 19.6 MeV was chosen for $^{68-78}$Se isotopic mass chain. The chosen energy window around the Fermi surface gives rise to a basis space $|\phi_\kappa\rangle$ in eq. (1), of the order of 67. For example, in ^{74}Se with the present choice of energy window the basis states from which good angular momentum states are chosen, consist of one 0-qp state, sixteen 2-qp neutron states, twenty-four 2-qp proton states and twenty-six (2-qp neutron+2-qp proton) 4-qp states. The basis deformation parameter ϵ_2

has been obtained by calculating the minima of potential energy state for $I = 0^+$ for $^{68-78}$Se. The values taken for ϵ_2 are given in table 1. In the present PSM calculation there is no mixing of intrinsic configurations arising from the prolate and oblate minima. In the present paper the prolate and oblate calculations have been taken independently.

3. Results and discussion

3.1 *Yrast spectra*

In table 1, we present the results of yrast spectra for $^{68-78}$Se. The yrast spectra have been obtained theoretically for two values of deformation parameters, one on oblate and the other on prolate side. The choice of the deformation parameters has been made from the calculation of potential energy surfaces (PES) for the 0^+ state. The deformation parameters chosen correspond to the minima of the potential energy surfaces on the prolate and oblate sides.

In the case of ^{68}Se, the oblate 0^+ state is found to be lower than the prolate 0^+ state by about 50 keV. Therefore, the low-lying states of the ground state band up to 6^+ can be compared with the corresponding energy states from the oblate band. After 6^+, it is observed that the energy states from the prolate band are much lower than the corresponding energy states of oblate yrast band. In figure 1a, the energy spectra for the yrast band in ^{68}Se is plotted as a function of spin and compared with the experimental yrast spectrum. It is very clear from the figure that for the higher angular momentum states $I \geq 8^+$ the prolate yrast spectrum shows much better agreement than the oblate yrast spectrum. However, for the low-lying states the oblate yrast spectrum is lower than the prolate yrast spectrum by very small energy difference hinting at the possibility of coexistence of oblate–prolate shapes in ^{68}Se.

Coming to ^{70}Se, it is noticed that the prolate yrast spectrum obtained for deformation $\epsilon_2 = 0.20$ is lower than the oblate yrast spectrum obtained for the deformation $\epsilon_2 = -0.20$. It is therefore the prolate yrast spectrum that can be compared with the yrast band. Comparison of the spectra is presented in figure 1b. It is noteworthy that the prolate yrast spectrum for higher angular momentum $I > 6^+$ is in much better agreement with the experiments. However, for the low-lying states no doubt the energies obtained from prolate minimum are less than those obtained from oblate minimum, but in comparison with experiments both can be considered to give satisfactory agreement hinting at the possibility of coexistence of shapes.

Similar observations can be made for ^{72}Se where the prolate minimum is lower and the spectra beyond 8^+ is in much better agreement with the experiments than the oblate yrast spectrum. The prolate and oblate minima have been obtained with $\epsilon_2 = 0.20$ and -0.21 respectively. For low-lying states again the results indicate the possibility of shape coexistence. In the case of ^{74}Se, the prolate minimum is obtained at $\epsilon_2 = 0.21$ and is lower than the corresponding oblate minimum obtained at $\epsilon_2 = -0.21$. The prolate yrast energies are in much better agreement than the corresponding oblate yrast spectrum. The disagreement with experiments for ^{74}Se is quite significant for the oblate yrast spectrum beyond 4^+ as is shown in figure 1d.

Table 1. The results of yrast energy spectra for $^{68-78}$Se. The symbols Exp., OYS, PYS and ϵ_2 stand for experiment, oblate yrast spectra, prolate yrast spectra and quadrupole deformation parameter respectively.

	Yrast spectra for ^{68}Se			Yrast spectra for ^{70}Se			Yrast spectra for ^{72}Se			Yrast spectra for ^{74}Se			Yrast spectra for ^{76}Se			Yrast spectra for ^{78}Se		
Spin (I)	Exp.	OYS $\epsilon_2=-0.24$	PYS $\epsilon_2=0.20$	Exp.	OYS $\epsilon_2=-0.20$	PYS $\epsilon_2=0.20$	Exp.	OYS $\epsilon_2=-0.21$	PYS $\epsilon_2=0.20$	Exp.	OYS $\epsilon_2=-0.21$	PYS $\epsilon_2=0.21$	Exp.	OYS $\epsilon_2=-0.22$	PYS $\epsilon_2=0.22$	Exp.	OYS	PYS $\epsilon_2=0.21$
0^+	0	0	0.05	0	0.12	0	0	0.17	0	0	0.22	0	0	0.11	0	0	–	0
2^+	0.853	0.78	0.98	0.94	1.02	0.86	0.86	0.88	0.84	0.63	0.79	0.69	0.55	0.61	0.53	0.63	–	0.49
4^+	1.94	1.91	2.25	2.03	2.18	1.98	1.63	1.95	1.87	1.36	1.78	1.59	1.33	1.44	1.40	1.51	–	1.33
6^+	3.30	3.35	3.70	3.03	3.61	3.30	2.46	3.30	3.09	2.23	3.12	2.69	2.26	2.36	2.47	2.56	–	2.44
8^+	4.75	5.02	4.55	4.03	4.60	4.03	3.42	4.37	3.70	3.19	4.12	3.50	3.26	3.04	3.34	3.60	–	3.36
10^+	5.96	6.95	5.62	5.20	6.58	5.10	4.50	5.92	4.78	4.25	4.97	4.38	4.29	3.88	4.36	4.63	–	4.41
12^+	7.33	8.82	7.03	6.51	8.54	6.54	5.70	7.79	6.33	5.44	6.32	5.50	5.43	5.11	5.53	5.78	–	5.47
14^+	8.82	10.97	8.17	7.94	10.51	7.59	7.03	9.56	7.51	6.73	7.94	6.8	–	–	–	–	–	–
16^+	9.87	13.04	9.08	9.43	12.45	8.39	8.49	11.47	8.20	8.11	9.85	8.16	–	–	–	–	–	–
18^+	11.04	15.23	10.44	10.64	14.38	9.67	10.09	13.61	9.41	9.67	11.98	9.50	–	–	–	–	–	–
20^+	12.79	17.46	12.30	12.26	16.40	11.42	11.83	15.78	11.09	11.35	14.38	10.80	–	–	–	–	–	–
22^+	15.18	19.88	14.52	14.25	18.72	13.54	13.74	18.28	13.13	13.11	16.91	12.70	–	–	–	–	–	–
24^+	18.07	22.59	17.24	16.49	21.42	16.13	15.90	21.06	15.71	14.91	19.62	14.98	–	–	–	–	–	–
26^+	21.20	25.56	20.56	19.21	24.62	19.40	18.21	24.06	18.93	–	–	–	–	–	–	–	–	–

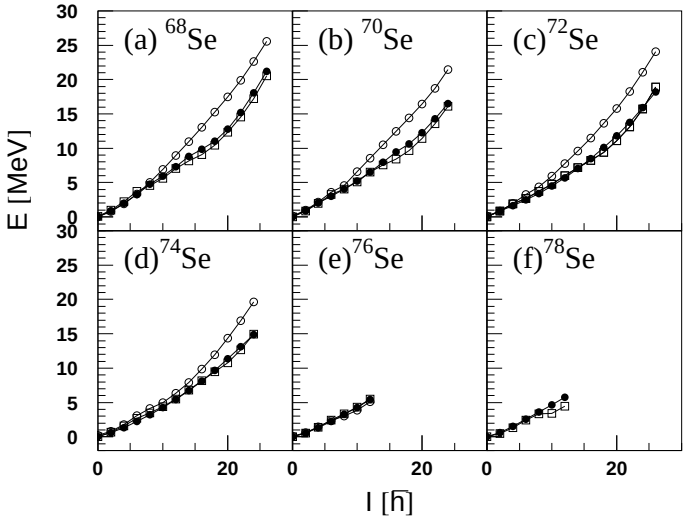

Figure 1. Comparison of calculated energies (open circle, oblate), (open square, prolate) $E(I)$ of the yrast bands with experimental data (filled circle) for $^{68-78}$Se. The calculated yrast bands consist of the lowest states after diagonalization at each angular momentum I.

In ^{76}Se, the prolate minimum is obtained for the deformation parameter $\epsilon_2 = 0.22$ and its energy is found to be lower than oblate minimum obtained at the deformation $\epsilon_2 = -0.22$ by 0.11 MeV. The low-lying states up to 4^+ obtained from the prolate minimum agree with the experimental yrast spectrum whereas the higher angular momentum states obtained from the oblate minimum are lower than their prolate counterparts. However, for these angular momentum states prolate spectrum is in much good agreement than oblate spectrum. In ^{78}Se, only one minimum is obtained on the prolate side for $\epsilon_2 = 0.21$. Comparison of this yrast spectrum shows good agreement up to 12^+.

3.2 *B(E2) reduced transition probabilities*

In table 2, we present the results of $B(E2)$ transition probabilities from $I \rightarrow I-2$ state for selenium isotopes. For ^{70}Se, the $B(E2)$ value of $2^+ \rightarrow 0^+$ is seen to be in satisfactory agreement with the experiments. In ^{72}Se, the $B(E2)$ transition values not only for $2^+ \rightarrow 0^+$ transition but also for higher transitions are reproduced within the limits of experimental error bars. In ^{74}Se, the values predicted by theory are less than the experimental values. However, in ^{76,78}Se, the values obtained from the prolate solution are in satisfactory agreement.

3.3 *Backbending phenomena*

In figure 2, the backbending plots for $^{68-78}$Se are presented. Here twice the moment of inertia (2θ) vs. square of rotational frequency (ω^2) is plotted. In each figure three

Table 2. Experimental (Exp.) and calculated (Th.) $B(E2)$ reduced transition probabilities (in units of e^2b^2). Columns 4 and 5 present the theoretical values of $B(E2)$ transitions obtained for oblate and prolate deformations, respectively. The effective charge is taken as 0.5. Experimental data for $B(E2)$s are taken from [12,16,20,24].

Nucleus $B(E2)$s	Transition $I_f^+ \to I_i^+$	Exp.	Th.	
			Oblate	Prolate
^{70}Se	$2_1 \to 0_1$	0.076(16)	0.042	0.049
^{72}Se	$2_1 \to 0_1$	$0.035(^{39}_{31})$	0.047	0.048
	$4_1 \to 2_1$	–	0.076	0.086
	$6_1 \to 4_1$	$0.085(^{92}_{78})$	0.089	0.097
	$8_1 \to 6_1$	–	0.000051	0.006
	$10_1 \to 8_1$	$0.163(^{84}_{45})$	0.0107	0.072
	$12_1 \to 10_1$	$0.152(^{87}_{27})$	0.033	0.080
	$14_1 \to 12_1$	$0.152(^{79}_{31})$	0.074	0.030
	$16_1 \to 14_1$	–	0.098	0.089
	$18_1 \to 16_1$	$0.129(^{72}_{02})$	0.095	0.093
	$20_1 \to 18_1$	$0.051(^{63}_{42})$	0.100	0.091
	$22_1 \to 20_1$	>0.045	0.055	0.090
^{74}Se	$2_1 \to 0_1$	0.074(0037)	0.050	0.054
	$4_1 \to 2_1$	–	0.077	0.093
	$6_1 \to 4_1$	0.218(0111)	0.087	0.103
	$8_1 \to 6_1$	0.180(0092)	0.0001	0.026
	$10_1 \to 8_1$	0.177(0148)	0.011	0.077
	$12_1 \to 10_1$	0.216(0277)	0.074	0.081
	$14_1 \to 12_1$	0.120(0166)	0.090	0.070
	$16_1 \to 14_1$	>0.070	0.098	0.030
^{76}Se	$2_1 \to 0_1$	0.083(0095)	0.056	0.064
	$4_1 \to 2_1$	0.133(0439)	0.080	0.102
^{78}Se	$2_1 \to 0_1$	0.065(0177)	–	0.059
	$4_1 \to 2_1$	0.095(0434)	–	0.091

curves are presented, one for experimental data, another for the prolate case and the third for the oblate case. In ^{68}Se, the experimental spectrum shows the onset of backbendings at 8^+ and 14^+. The first backbending appears at 8^+ whereas the second backbending appears at 14^+. The yrast spectrum arising from oblate minimum in the nucleus shows slight backbending at 12^+. However, the backbending plot obtained for prolate yrast spectrum shows two distinct backbendings, the first backbending at 6^+ and the second backbending at 12^+. From the comparison of calculated results with the observed results, it appears that the prolate backbending plot agrees qualitatively much better than the backbending plot arising from oblate deformation with the experiments. As said earlier, in this nucleus the yrast energies arising from the prolate minima for the higher angular momentum states are found

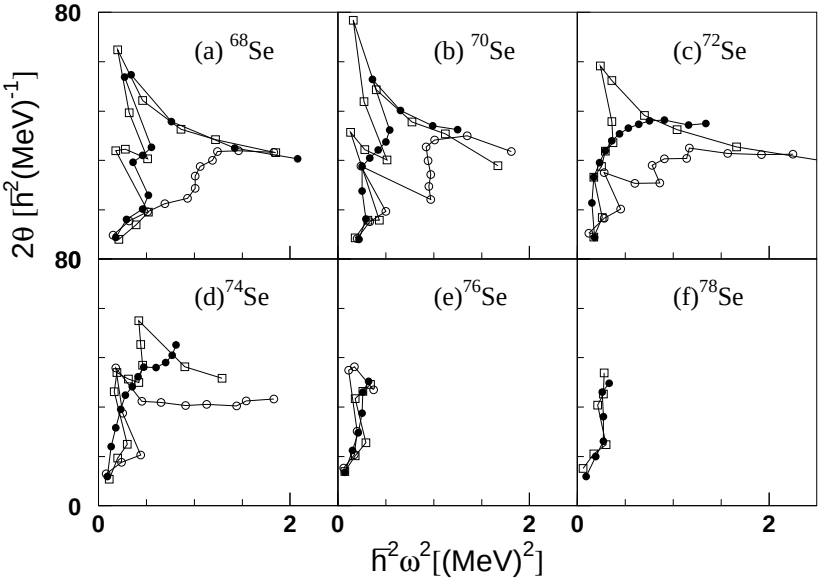

Figure 2. Comparison of calculated moments of inertia (open circle, oblate), (open square, prolate), 2θ with experimental data (filled circle) as a function of rotational frequency ω^2 for $^{68-78}$Se. These quantities are defined as $2\theta = \frac{2I-1}{\omega}$, $\omega = [E(I) - E(I-2)]/2$.

to be lower than the corresponding energy values arising from oblate minima. However, the low-lying states arising from the oblate minimum were found to be lower than the corresponding prolate energies. The backbending in this nucleus could be arising due to change of shape from oblate to prolate as we move higher along the yrast states. In ^{70}Se, the manifestation of first backbending takes place at 4^+ and second backbending at 16^+. The backbending plot arising from prolate yrast spectrum shows first backbending at 6^+ and second backbending at 12^+. The backbending plot arising from the oblate yrast spectrum shows the first backbending at 6^+ and the second backbending at 10^+. For this nucleus the backbending plot arising from prolate yrast spectrum is noticed to be in agreement with experiments. In ^{72}Se, the experimental spectrum shows very gradual backbending at 2^+. This is reproduced by the prolate yrast spectrum at 4^+. This spectrum shows another backbending at 12^+ which is not exhibited by experimental yrast spectrum. The oblate yrast spectrum also shows two backbendings, the first one appears at 6^+ and the second one at 12^+. In the case of ^{74}Se, experimentally there is no backbending but the yrast spectrum arising from the prolate spectrum shows one backbending at 6^+. However, the backbending plot arising from prolate yrast spectrum is in better agreement qualitatively. In the case of ^{76}Se, experimentally there is no backbending. However, the prolate and oblate backbending plots show one backbending in this nucleus. In ^{78}Se, the experimental spectrum show backbending at 6^+. This is reproduced by the prolate yrast spectrum at 6^+.

It is understood that in spin range where the onset of backbending takes place, it should be marked by the crossing of ground state band by other bands. Band

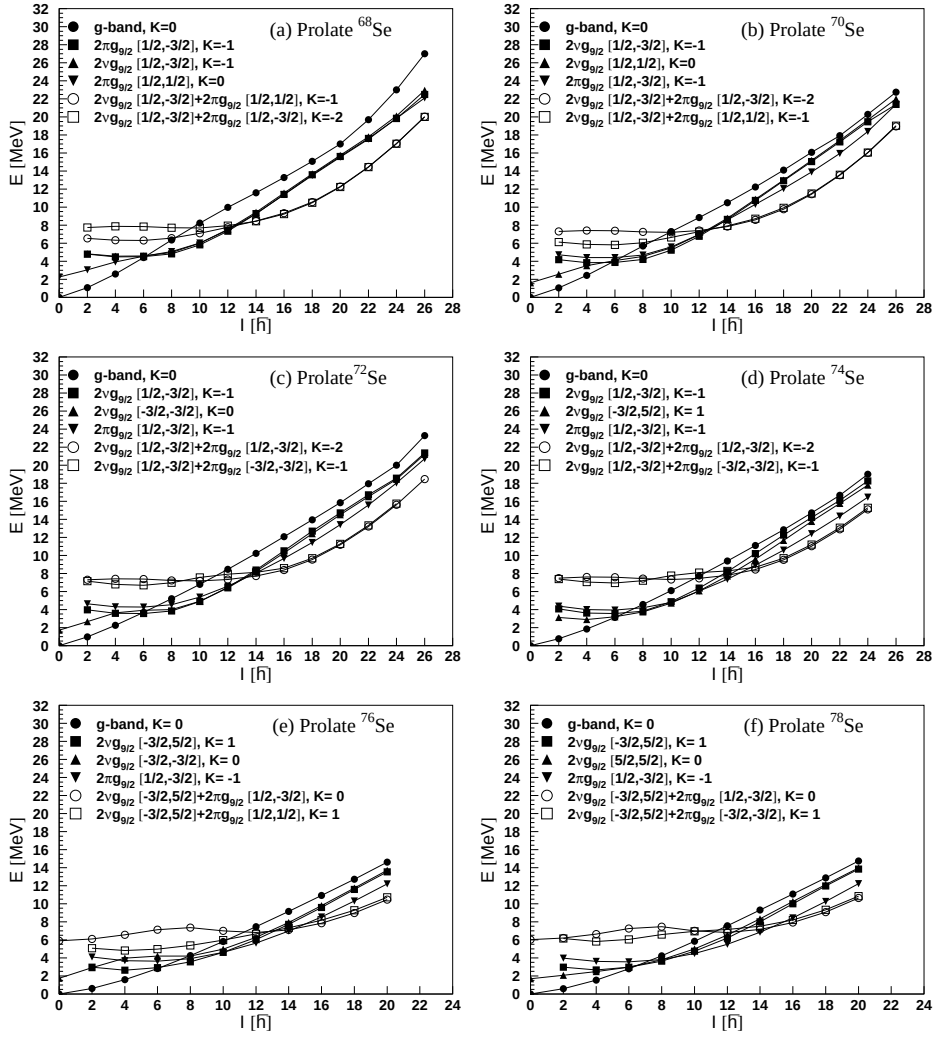

Figure 3. Band diagrams for $^{68-78}$Se for prolate deformation.

crossing occurs in a majority of nuclei irrespective of whether they show a backbending or not (up-bending). The band that crosses the g-band is referred to as s-band. A backbending occurs [46] if the crossing angle between two bands is large. Otherwise up-bending occurs. If the crossing angle is large, the g- and s-bands do not admix each other except at the nearest vicinity of the crossing point because they are mostly well-separated energetically from each other. Therefore, the transition from the g-band to s-band takes place suddenly. This results in the backbending effect. On the other hand, if the crossing angle is small, the g- and s-bands will stay close to each other for a relatively large spin interval so that they can easily admix with each other all the way and, therefore, the transition between them occurs gradually. This is up-bending.

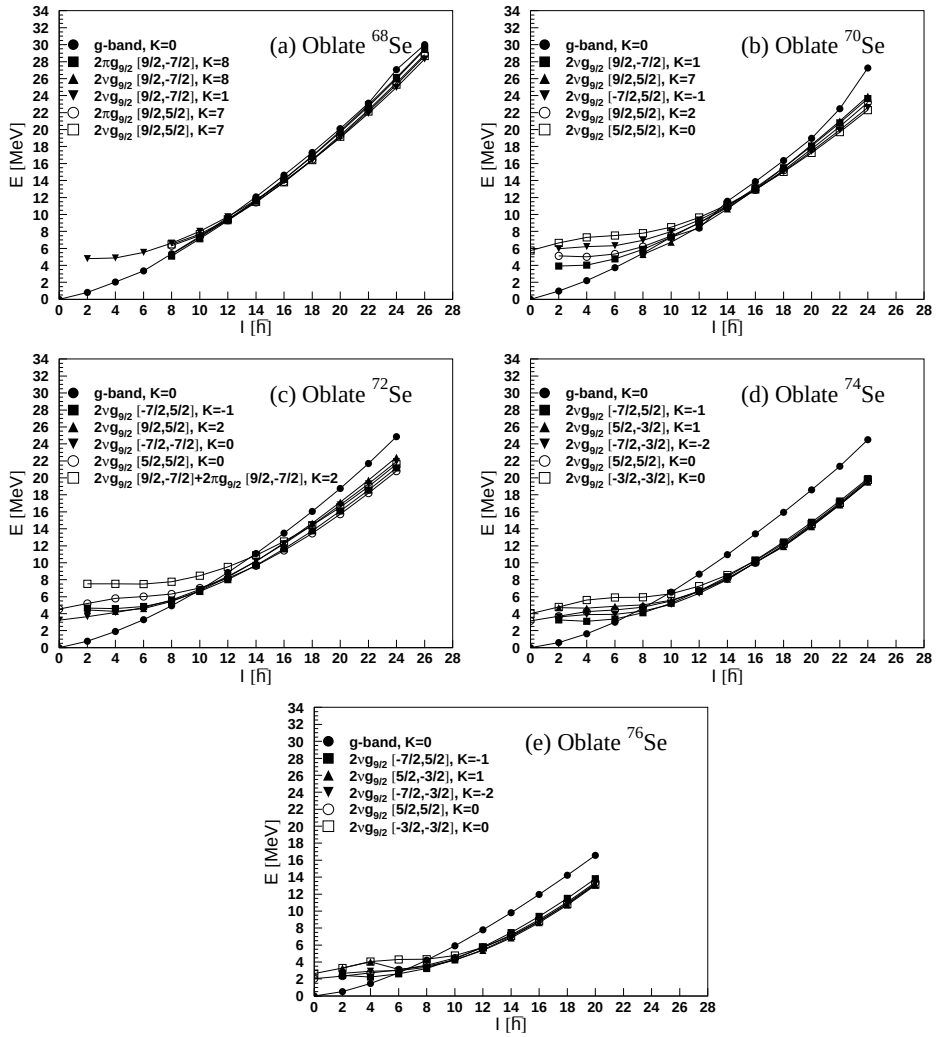

Figure 4. Band diagrams for $^{68-76}$Se for oblate deformation.

Figure 3a represents the band diagram of ^{68}Se for the prolate deformation. It is evident from this figure that at spin $6\hbar$ the ground state band is crossed by three 2-qp bands having configurations $2\pi g_{9/2}(1/2,-3/2)$, $K=-1$, $2\nu g_{9/2}(1/2,-3/2)$, $K=-1$, $2\pi g_{9/2}(1/2,1/2)$, $K=0$. This band crossing could be linked to the occurrence of backbending in the observed yrast spectrum at $8\hbar$ which is reproduced by the prolate yrast spectrum at $6\hbar$. The second band crossing in the prolate band diagram could be responsible for the onset of second backbending in the observed yrast spectrum. The second backbending observed at $14\hbar$, that is reproduced by prolate spectrum at $12\hbar$ arises due to the crossing of two 4-qp bands having configurations $2\nu g_{9/2}(1/2,-3/2)+2\pi g_{9/2}(1/2,1/2)$, $K=-1$ and

Table 3. Comparison of calculated (Th.) g-factors with experimental (Exp.) and IBM-II values for $^{68-78}$Se isotopes. Data taken from refs [20,35].

				Th.	
Nucleus	g(I)	Exp.	IBM-II	Oblate	Prolate
^{68}Se	$g(2_1)$	–	–	0.401	0.436
	$g(4_1)$	–	–	0.440	0.454
	$g(6_1)$	–	–	0.458	0.287
	$g(8_1)$	–	–	0.555	0.124
^{70}Se	$g(2_1)$	–	–	0.404	0.398
	$g(4_1)$	–	–	0.416	0.381
	$g(6_1)$	–	–	0.399	0.184
	$g(8_1)$	–	–	−0.286	−0.098
^{72}Se	$g(2_1)$	–	–	0.378	0.332
	$g(4_1)$	–	–	0.384	0.299
	$g(6_1)$	–	–	0.369	0.261
	$g(8_1)$	–	–	−0.284	−0.207
^{74}Se	$g(2_1)$	0.428(27)	0.239	0.334	0.240
	$g(4_1)$	0.50(10)	–	0.349	0.220
	$g(6_1)$	–	–	0.332	0.180
	$g(8_1)$	–	–	−0.282	−0.196
^{76}Se	$g(2_1)$	0.403(23)	0.125	0.272	0.184
	$g(4_1)$	0.64(9)	–	0.225	0.201
	$g(6_1)$	–	–	0.026	0.206
	$g(8_1)$	–	–	−0.133	−0.0775
^{78}Se	$g(2_1)$	0.384(25)	0.070	–	0.102
	$g(4_1)$	0.39(12)	–	–	0.112
	$g(6_1)$	–	–	–	0.134
	$g(8_1)$	–	–	–	−0.192

$2\nu g_{9/2}(1/2,-3/2)+2\pi g_{9/2}(1/2,-3/2)$, $K=-2$. In figure 4a, the band diagram for ^{68}Se by taking oblate minimum is displayed. At 8^+ the ground state band is crossed by $2\pi g_{9/2}(9/2,-7/2)$, $K=8$ band which could be resulting in the onset of backbending in oblate yrast spectrum. As is evident from figure 2b, in ^{70}Se, one observes that there are two backbendings exhibited by the observed yrast spectrum. The first backbending is observed at $4\hbar$ and second backbending at $16\hbar$. From the same figure one notes that first backbending arises from prolate minimum at $6\hbar$ and second backbending at $12\hbar$. Figure 3b represents the band diagram for ^{70}Se by taking prolate deformation. It indicates that in the spin range $6\hbar$–$8\hbar$, the ground state band is crossed by three 2-qp bands having configurations $2\nu g_{9/2}(1/2,-3/2)$, $K=-1$, $2\nu g_{9/2}(1/2,1/2)$, $K=0$, $2\pi g_{9/2}(1/2,-3/2)$, $K=-1$. However, in the spin range $12\hbar$–$14\hbar$ there occurs the crossing of two 4-qp bands having configurations $2\nu g_{9/2}(1/2,-3/2)+2\pi g_{9/2}(1/2,-3/2)$, $K=-2$ and $2\nu g_{9/2}(1/2,-3/2)+2\pi g_{9/2}(1/2,1/2)$, $K=-1$. In figure 4b, the band

diagram for ^{70}Se, obtained for oblate minimum is shown. This band diagram shows one band crossing at $8\hbar$ and another at $12\hbar$. The band crossing at $8\hbar$ arises due to the crossing of one 2-qp band having configuration $2\nu g_{9/2}(9/2, 5/2)$, $K = 7$ and another crossing at $12\hbar$ arises due to four 2-qp bands having configurations $2\nu g_{9/2}(9/2, -7/2)$, $K = 1$, $2\nu g_{9/2}(-7/2, 5/2)$, $K = -1$, $2\nu g_{9/2}(9/2, 5/2)$, $K = 2$, $2\nu g_{9/2}(5/2, 5/2)$, $K = 0$. In ^{72}Se, one observes that only one backbending is exhibited by the observed yrast spectrum at $2\hbar$ as is evident from figure 2c. However, second backbending is not exhibited by the observed yrast spectrum. From the same figure, one notes that there are two backbendings exhibited by the prolate yrast spectrum at $4\hbar$ and $12\hbar$. Figure 3c represents the band diagram for ^{72}Se, obtained by taking prolate deformation. It indicates that in spin range $6\hbar$, the ground state band is crossed by three 2-qp bands having configurations $2\nu g_{9/2}(1/2, -3/2)$, $K = -1$, $2\nu g_{9/2}(-3/2, -3/2)$, $K = 0$ and $2\pi g_{9/2}(1/2, -3/2)$, $K = -1$. However, in the spin range $12\hbar$–$14\hbar$ there occurs the crossing of two 4-qp bands having configurations $2\nu g_{9/2}(1/2, -3/2)+2\pi g_{9/2}(1/2, -3/2)$, $K = -2$ and $2\nu g_{9/2}(1/2, -3/2)+2\pi g_{9/2}(1/2, 1/2)$, $K = -1$. In figure 4c, the band diagram for ^{72}Se obtained for oblate minimum is shown. This band diagram shows only one band crossing at $10\hbar$ due to the crossing of four 2-qp bands having configurations $2\nu g_{9/2}(-7/2, 5/2)$, $K = -1$, $2\nu g_{9/2}(9/2, 5/2)$, $K = 2$, $2\nu g_{9/2}(-7/2, -7/2)$, $K = 0$ and $2\nu g_{9/2}(5/2, 5/2)$, $K = 0$.

In ^{74}Se, backbending is not exhibited by the observed yrast spectrum as is evident from figure 2d. However, from the same figure one notes that the first backbending arising from the prolate and oblate spectra occurs at $8\hbar$. Figure 3d represents the band diagram for ^{74}Se, by taking prolate deformation. It indicates that in the spin range $6\hbar$–$8\hbar$, the ground state band is crossed by three 2-qp bands having configurations $2\nu g_{9/2}(1/2, -3/2)$, $K = -1$, $2\nu g_{9/2}(-3/2, 5/2)$, $K = 1$ and $2\pi g_{9/2}(1/2, -3/2)$, $K = -1$. In the spin range $14\hbar$–$16\hbar$ there occurs the crossing of two 4-qp bands having configurations $2\nu g_{9/2}(1/2, -3/2)+2\pi g_{9/2}(1/2, -3/2)$, $K = -2$ and $2\nu g_{9/2}(1/2, -3/2)+2\pi g_{9/2}(-3/2, -3/2)$, $K = -1$. In figure 4d, the band diagram for ^{74}Se obtained by taking oblate deformation is shown. The band diagram shows band crossing around spin $8\hbar$ due to crossing of five 2-qp bands having configurations $2\nu g_{9/2}(-7/2, 5/2)$, $K = -1$, $2\nu g_{9/2}(5/2, -3/2)$, $K = 1$, $2\nu g_{9/2}(-7/2, -3/2)$, $K = -2$, $2\nu g_{9/2}(5/2, 5/2)$, $K = 0$ and $2\nu g_{9/2}(-3/2, -3/2)$, $K = 0$.

In ^{76}Se, the observed yrast spectrum is available up to $12\hbar$. Backbending is not exhibited by the observed yrast spectrum as is evident from figure 2e. However, from the same figure one notes that both prolate and oblate spectra show backbending at $8\hbar$. Figure 3e represents the band diagram for ^{76}Se, by taking prolate deformation. The diagram shows first band crossing in the spin range $6\hbar$–$8\hbar$, with three 2-qp bands having configurations $2\nu g_{9/2}(-3/2, 5/2)$, $K = 1$, $2\nu g_{9/2}(-3/2, -3/2)$, $K = 0$ and $2\pi g_{9/2}(1/2, -3/2)$, $K = -1$ crossing the ground state band. The second band crossing is observed to take place at the spin $14\hbar$ with two 4-qp bands having configurations $2\nu g_{9/2}(-3/2, 5/2)+2\pi g_{9/2}(1/2, -3/2)$, $K = 0$ and $2\nu g_{9/2}(-3/2, 5/2)+2\pi g_{9/2}(1/2, 1/2)$, $K = 1$ becoming yrast. In figure 4e, the band diagram for ^{76}Se, obtained by taking oblate deformation is shown. This band diagram shows band crossing in the spin range $6\hbar$–$8\hbar$ due to crossing of five 2-qp bands having configurations $2\nu g_{9/2}(-7/2, 5/2)$, $K = -1$, $2\nu g_{9/2}(5/2, -3/2)$, $K = 1$,

$2\nu g_{9/2}(-7/2,-3/2)$, $K=-2$, $2\nu g_{9/2}(5/2,5/2)$, $K=0$ and $2\nu g_{9/2}(-3/2,-3/2)$, $K=0$.

In ^{78}Se, the observed yrast spectrum is available up to $12\hbar$. The observed yrast spectrum shows backbending at $8\hbar$. In figure 3f, the band diagram for prolate solution is displayed. The diagram shows first band crossing in the spin range $6\hbar$–$8\hbar$ with three 2-qp bands having configurations $2\nu g_{9/2}(5/2,-3/2)$, $K=1$, $2\nu g_{9/2}(5/2,5/2)$, $K=0$ and $2\pi g_{9/2}(1/2,-3/2)$, $K=-1$ crossing the ground state band. The second band crossing is observed to take place in the spin range $14\hbar$–$16\hbar$ with two 4-qp bands having configurations $2\nu g_{9/2}(-3/2,5/2)+2\pi g_{9/2}(1/2,-3/2)$, $K=0$ and $2\nu g_{9/2}(-3/2,5/2)+2\pi g_{9/2}(-3/2,-3/2)$, $K=1$ becoming yrast.

3.4 *g-factors*

In table 3, the calculated results on g-factors along with the available experimental values and also those predicted by IBM-II model [35] are presented. Experimentally, the g-factors for 2_1^+ state show a decreasing trend with increase in mass number. This trend is reproduced by the calculated $g(2_1^+)$ values. Our calculated results are relatively better than those predicted by IBM-II calculations. Experimentally, ^{78}Se is observed to have the least $g(2_1^+)$ value. The calculated value of $g(2_1^+)$ obtained from PSM calculations also show least value for ^{78}Se.

4. Conclusions

From the presentation and discussion of results, the following broad conclusions can be drawn:

1. The PSM calculations carried out with quadrupole-quadrupole interaction plus monopole plus quadrupole pairing force gives a good overall description of $^{68-78}$Se isotopic mass chain.
2. The calculations indicate oblate deformation for low-lying states and prolate deformation for higher lying states in ^{68}Se isotope.
3. The calculations confirm the occurrence of two backbending in ^{68,70}Se and one in ^{78}Se.
4. The cause of backbending in ^{68}Se is oblate–prolate shape transition and crossing of bands.
5. The calculations indicate prolate deformation for the yrast bands in $^{70-78}$Se.

Acknowledgements

The discussions and collaborations with Prof. J A Sheikh and Y Sun are deeply acknowledged.

References

[1] S M Fischer, D P Balamuth, P A Hausladen, C J Lister, M P Carpenter, D Seweryniak and J Schwartz, *Phys. Rev. Lett.* **84**, 4064 (2000)
[2] S M Fischer, C J Lister and D P Balamuth, *Phys. Rev.* **C67**, 064318 (2003)
[3] R M Leider and J Drapper, *Phys. Rev.* **C2**, 531 (1970)
[4] J H Hamilton, A V Ramayya, W T Pinkston, R M Ronningen, G Garcia-Bermudez, R L Robinson, H J Kim, R O Sayer and H K Carter, *Phys. Rev. Lett.* **32**, 239 (1974)
[5] M L Halbert, P O Tjon, I Espe, G B Hagemann and B Herskind, *Nucl. Phys.* **A259**, 496 (1976)
[6] R M Ronningen, A V Ramayya, J H Hamilton, W Lourens, J Lange, H K Carter and R O Sayer, *Nucl. Phys.* **A261**, 439 (1976)
[7] R B Piercey, A V Ramayya, R M Ronningen, J H Hamilton, R L Robinson and H J Kim, *Phys. Rev. Lett.* **37**, 496 (1976)
[8] K P Lieb and J J Kolata, *Phys. Rev.* **C15**, 939 (1977)
[9] R B Piercey, A V Ramayya, R M Ronningen, J H Hamilton, V Maruhn-Rezwani, R L Robinson and H J Kim, *Phys. Rev.* **C19**, 1344 (1979)
[10] C J Gross, P D Cottle, D M Headly, U J Huttmeier, E F Moore and S L Tab, *Phys. Rev.* **C36**, 2127 (1987)
[11] J Adam, M Honusek, A Spalek, D N Doynikov, A D Efimov, M F Kodojavov, I Kh Lamberg, A A Pasternak, O K Vorov and U Y Zhovliev, *Z. Phys.* **A332**, 143 (1989)
[12] P D Cottle, J W Holocomb, T D Johnson, K A Stuckey, S L Tabor, P C Womble, S G Buccino and F E Durham, *Phys. Rev.* **C42**, 1254 (1990)
[13] A M Hurst *et al, Phys. Rev. Lett.* **98**, 072501 (2007)
[14] B S Nara Singh *et al, Phys. Rev.* **C75**, 061301(R) (2007)
[15] T Mylaeus *et al, J. Phys.* **G15**, L135 (1989)
[16] R Palit, H C Jain, P K Joshi, J A Sheikh and Y Sun, *Phys. Rev.* **C63**, 024313 (2001)
[17] R Palit, H C Jain, P K Joshi and J A Sheikh, *Pramana – J. Phys.* **57**, 191 (2001)
[18] J Doring, G D Johns, M A Riley, S L Tabor, Y Sun and J A Sheikh, *Phys. Rev.* **C57**, 2912 (1998)
[19] G Rainovski *et al*, *J. Phys. G: Nucl. Part. Phys.* **28**, 2617 (2002)
[20] K H Speidel, N Benczer- Koller, G Kumbartzki, C Barton and A Gelberg, *Phys. Rev.* **C57**, 2181 (1998)
[21] T Hayakawa *et al, Phys. Rev.* **C67**, 064310 (2003)
[22] T Matsuzaki and H Taketani, *Nucl. Phys.* **A390**, 413 (1982)
[23] J C Wells Jr, R L Robinson, H J Kim, R O Sayer, R B Piercey, A V Ramayya, J H Hamilton and C F Maguire, *Phys. Rev.* **C22**, 1126 (1980)
[24] J Heese, K P Lieb, L Luhmann, F Raether, B Wormann, D Alber, H Grawe, J Eberth and T Mylaeus, *Z. Phys.* **A325**, 45 (1986)
[25] B Singh, *Nucl. Data Sheets* **105**, 267 (2005)
[26] T W Burrows, *Nucl. Data Sheets* **97**, 1 (2002)
[27] J K Tuli, *Nucl. Data Sheets* **103**, 389 (2004)
[28] W T Chou and M M King, *Nucl. Data Sheets* **73**, 215 (1994)
[29] A R Farhan, *Nucl. Data Sheets* **74**, 529 (1995)
[30] B Singh, *Nucl. Data Sheets* **74**, 63 (1995)
[31] S Rab, *Nucl. Data Sheets* **63**, 1 (1991)
[32] Y Sun, *Euro. Phys. J.* **A20**, 133 (2004)
[33] A V Afnasjev and S Frauendorf, *Phys. Rev.* **C71**, 064318 (2005)
[34] P N Tripathi and S K Sharma, *Phys. Rev.* **C34**, 1081 (1986)

[35] T J Mertzimekis, A E Stuchbery, N Benczor- Koller and M J Taylor, *Phys. Rev.* **C68**, 054304 (2003)
[36] R Alvarez-Rodriguez, P Sarriguren, E M de Guerra, L Pacearescu, A Faessler and F Simkovic, *Phys. Rev.* **C70**, 064309 (2004)
[37] A Petrovici, K W Schmid, F Grummer and A Faessler, *Nucl. Phys.* **A517**, 108 (1990); **A504**, 277 (1989)
[38] A Petrovici, K W Schmid, F Grummer, A Faessler and T Haribata, *Nucl. Phys.* **A483**, 317 (1988)
[39] A V Afanasjev, D B Fossan, G J Lane and I Ragnarsson, *Phys. Rep.* **322**, 1 (1999)
[40] W Nazarewicz, J Dude, R Bengtsson, T Bengtsson and I Ragnarsson, *Nucl. Phys.* **A435**, 397 (1985)
[41] T A War, A Chandhan, R Devi, A Bharti and S K Khosa, *Ind. J. Pure and Appl. Phys.* **41**, 914 (2003)
[42] K Hara and Y Sun, *Int. J. Mod. Phys.* **E4**, 637 (1995)
[43] Y Sun and D H Feng, *Phys. Rep.* **264**, 375 (1996)
[44] Y Sun and J L Edigo, *Nucl. Phys.* **A580**, 1 (1994)
[45] T Bengtsson and I Ragnarsson, *Nucl. Phys.* **A436**, 14 (1985)
[46] K Hara and Y Sun, *Nucl. Phys.* **A529**, 445 (1991)